Near-infrared fluorescent sensor for in vivo copper imaging in a murine Wilson disease model

Tasuku Hirayama[a,1], Genevieve C. Van de Bittner[a,1], Lawrence W. Gray[b], Svetlana Lutsenko[b], and Christopher J. Chang[a,c,2]

[a]Department of Chemistry, and [c]Howard Hughes Medical Institute, University of California, Berkeley, CA 94720; and [b]Department of Physiology, The Johns Hopkins University, Baltimore, MD 21205

Edited by Harry B. Gray, California Institute of Technology, Pasadena, CA, and approved December 20, 2011 (received for review August 22, 2011)

Copper is an essential metal nutrient that is tightly regulated in the body because loss of its homeostasis is connected to severe diseases such as Menkes and Wilson diseases, Alzheimer's disease, prion disorders, and amyotrophic lateral sclerosis. The complex relationships between copper status and various stages of health and disease remain challenging to elucidate, in part due to a lack of methods for monitoring dynamic changes in copper pools in whole living organisms. Here we present the synthesis, spectroscopy, and in vivo imaging applications of Coppersensor 790, a first-generation fluorescent sensor for visualizing labile copper pools in living animals. Coppersensor 790 combines a near-infrared emitting cyanine dye with a sulfur-rich receptor to provide a selective and sensitive turn-on response to copper. This probe is capable of monitoring fluctuations in exchangeable copper stores in living cells and mice under basal conditions, as well as in situations of copper overload or deficiency. Moreover, we demonstrate the utility of this unique chemical tool to detect aberrant increases in labile copper levels in a murine model of Wilson disease, a genetic disorder that is characterized by accumulation of excess copper. The ability to monitor real-time copper fluxes in living animals offers potentially rich opportunities to examine copper physiology in health and disease.

molecular imaging | near-infrared fluorophore | metal homeostasis | diagnostic

Copper is an essential element for life, and maintaining its proper homeostasis is critical for the growth, development, and fitness of living organisms (1–7). Indeed, loss of copper homeostasis in the body has severe consequences owing to its potent redox activity, which, if uncontrolled, can lead to aberrant oxidative and nitrosative stress events that accompany diseases ranging from cancer (8) to cardiovascular disorders (9–11) to Alzheimer's and related neurodegenerative diseases (4, 12–18). Moreover, genetic inactivation of the obligatory copper-handling proteins ATP7A, ATP7B, and SCO1/2 results in serious afflictions (19) of copper deficiency (Menkes disease) (20, 21), copper overload (Wilson disease) (14, 22), and mitochondrial dysfunction (23), respectively, which can be lethal if left untreated.

Given the central importance of copper to human health and disease, creation of technologies that allow selective and sensitive monitoring of exchangeable copper stores in living systems can help disentangle the global physiological and/or pathological consequences of copper regulation (4, 24–26). To meet this goal, our laboratory and others have devised small-molecule (27–35), protein (36, 37), and nucleic acid (38, 39) fluorescent sensors for visualizing labile copper pools in biological contexts. Such chemical tools have provided fundamental insights into the biology of copper, including calcium-dependent copper translocation in neurons (32), antimicrobial behavior of copper surfaces (40, 41), as well as prioritization of mitochondrial copper pools in patient cells with synthesis of cytochrome c oxidase (SCO) mutations (33). However, these studies have been largely limited to dissociated cell cultures and other thin specimens owing to the need for ultraviolet or visible wavelength excitation. As such, the translation of copper detection methodologies to in vivo imaging in mammalian models of health and disease remains a significant and difficult challenge.

We now report the synthesis, spectroscopic properties, and biological imaging applications of Coppersensor 790 (CS790), a first-generation fluorescent sensor for visualizing exchangeable copper stores in living animals. CS790 exhibits a selective and sensitive turn-on response to Cu^+ and features near-IR excitation and emission profiles ideal for penetration through thicker biological specimens. Moreover, we establish the ability of CS790 to monitor fluctuations in labile copper levels in living cells, and demonstrate that this chemical tool can be used to detect exchangeable copper stores in living mice under basal, copper-overload, or copper-deficient conditions. Finally, we apply CS790 imaging to interrogate aberrant copper accumulation in a murine model of Wilson disease, highlighting the potential diagnostic value of this technology. Taken together, these data provide a starting point for using molecular imaging to explore the chemistry and biology of copper at the in vivo level.

Results and Discussion

Design and Synthesis of CS790. In designing a turn-on fluorescent sensor for in vivo copper detection, we sought to utilize a photoinduced electron transfer (PET) mechanism for copper sensing on a dye scaffold compatible with live-animal imaging. For the latter, we chose a cyanine 7 (Cy7) dye as the optical reporter. This fluorophore platform possesses near-IR absorption and emission profiles to maximize tissue penetration of the fluorescent signal from the dye while minimizing native tissue autofluorescence, in addition to being biologically inert, nontoxic, and compatible with aqueous media (42, 43). Moreover, related probes for nitric oxide and pH show that the fluorescence properties of Cy7-type dyes can be modulated by PET (44–49). As such, we reasoned that installing an electron-rich 9-aza-2,6,13-trithiapentadecane receptor in appropriate proximity to a Cy7 scaffold would produce a sensor that is responsive to Cu^+, the dominant oxidation state for this metal in cells. As indicated in previous reports, utilization of a soft sulfur-rich receptor provides an appropriate Pearson acid-base match for the soft Cu^+ ion (27, 28, 31–33, 50, 51). Fig. 1 summarizes the synthesis of CS790 from the convergent coupling of appropriately derivatized Cy7 and receptor building blocks.

Spectroscopic Characterization of CS790. Initial spectroscopic characterization of CS790 verified a shift in excitation and emission

Author contributions: T.H., G.C.V.d.B., L.W.G., S.L., and C.J.C. designed research; T.H., G.C.V.d.B., and L.W.G. performed research; T.H., G.C.V.d.B., L.W.G., and S.L. contributed new reagents/analytic tools; T.H., G.C.V.d.B., L.W.G., S.L., and C.J.C. analyzed data; and T.H., G.C.V.d.B., and C.J.C. wrote the paper.

The authors declare no conflict of interest.

This article is a PNAS Direct Submission.

[1]T.H. and G.C.V.d.B. contributed equally to this work.

[2]To whom correspondence should be addressed. E-mail: chrischang@berkeley.edu.

This article contains supporting information online at www.pnas.org/lookup/suppl/doi:10.1073/pnas.1113729109/-/DCSupplemental.

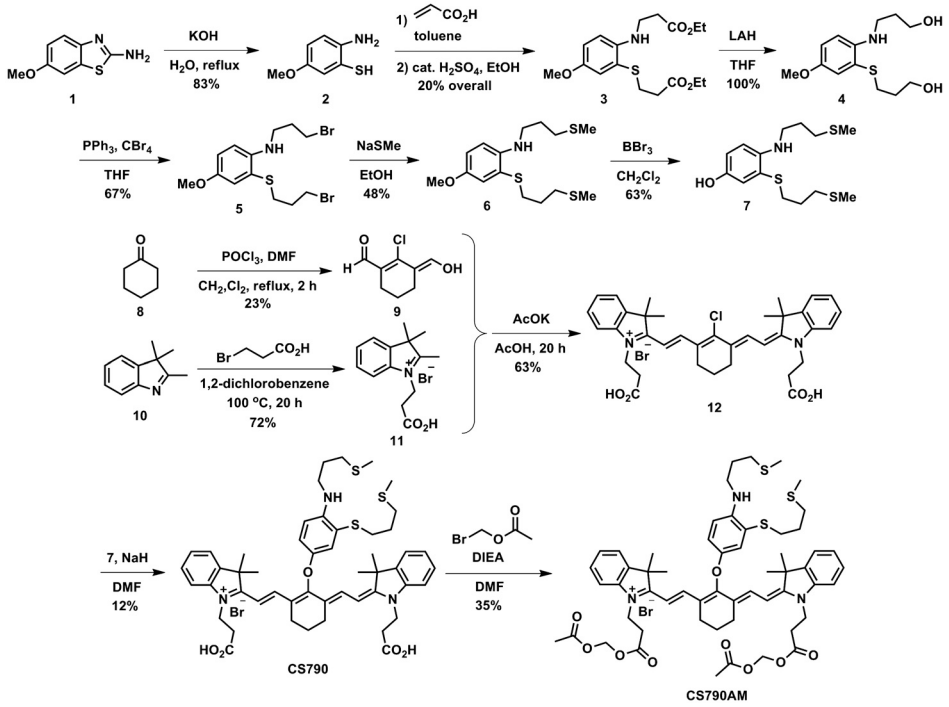

Fig. 1. Synthesis of Coppersensor 790 (CS790) and Coppersensor 790 Acetoxymethyl Ester (CS790AM).

profiles from the visible region to the near-IR window, with maximal absorption of apo and Cu^+-bound CS790 centered at 760 nm (Fig. S1) and maximal emission centered at 790 nm (Fig. 2). In response to Cu^+, CS790 shows a 15-fold enhancement in fluorescence intensity (Fig. S1), corresponding to a quantum yield increase from $\Phi = 0.0042$ for the apo dye to $\Phi = 0.072$ for the copper-bound sensor. Binding analysis using the method of continuous variation (Job's plot, Fig. 2) establishes a 1 : 1 binding stoichiometry between CS790 and Cu^+ with an apparent dissociation constant (K_d) of 3.0×10^{-11} M (Fig. S1). Importantly, selectivity tests with various biologically relevant metals indicate that CS790 does not give false positives to other metals at cellular concentrations, nor do these metals interfere with the Cu^+-triggered turn-on response (Fig. 2). Additionally, the fluorescent emissions of apo and Cu^+-bound CS790 are stable over the physiological pH range, with a $pK_a < 2.0$ for apo CS790 (Fig. S1). The unique combination of near-IR excitation/emission profiles on a biologically compatible fluorophore platform, a robust turn-on response, as well as the tight, sensitive, and selective binding of Cu^+, presage the successful application of CS790 for detection of labile copper stores in living systems.

CS790AM Detects Changes in Labile Copper Levels in Living Cells. Following characterization of the spectroscopic properties of CS790, we sought to apply this sensor to image fluctuations in exchangeable copper pools in living cells. As live cells possess highly lipophilic membranes, we transformed the carboxy groups of CS790 into acetoxymethyl esters to form CS790AM (Fig. 1), which, unlike CS790, is able to accumulate within cells (52, 53) (Fig. S2). Once inside the cell, CS790AM is de-esterified by intracellular esterases to produce CS790 (Fig. S3). Unveiling of the negatively charged carboxylates helps trap CS790 within the cell, as demonstrated by the limited loss of fluorescent signal in HEK 293T cells over an hour (Fig. S4). After performing this initial characterization of CS790AM, we utilized two complementary techniques, flow cytometry and confocal microscopy, for CS790-based copper detection in living cells. Flow cytometry experiments in HEK 293T cells reveal a marked shift in population distribution from low fluorescence intensity to high fluorescence intensity when cells are supplemented with copper salts (Fig. 3). Moreover, treatment of copper-supplemented cells with a copper chelator, tris[2(ethylthio)ethyl]amine (NS3′), reverted the cells to a low fluorescent intensity population. Taken together, the data establish the capacity of CS790AM to detect fluctuations in labile copper levels in living cells and demonstrate that this sensor can monitor both increases and decreases in exchangeable copper in a reversible manner.

With flow cytometry data in hand, CS790AM was used for confocal imaging experiments to further verify its capabilities to detect intracellular exchangeable copper and provide subcellular spatial resolution. In agreement with the flow cytometry results, CS790AM-stained HEK 293T cells show a low intracellular fluorescence, whereas their copper-supplemented counterparts display a marked increase in fluorescence (Fig. 3). In addition, treatment of copper-supplemented cells with NS3′ restores intracellular fluorescence to baseline levels, again consistent with reversible Cu^+ binding to the sensor.

CS790AM Visualizes Dynamic Changes in Exchangeable Copper Stores in Living Mice. We next sought to apply CS790AM to the in vivo monitoring of labile copper stores in living mice. These experiments utilized a sensitive CCD camera to image mice under basal conditions, as well as during copper overload or depletion. Initial studies focused on five different treatment conditions, aiming to establish the ability of CS790AM to detect fluctuations of exchangeable copper pools in hairless SKH-1 mice. First, we verified the low level of autofluorescence from mice following near-IR excitation by imaging mice injected with vehicle alone (Fig. 4). Then, to determine the basal level of signal from CS790AM in vivo, mice were treated with CS790AM and the fluorescence output was monitored 5 min after dye injection (Fig. 4). In vivo copper detection by CS790AM was established using a third group of mice, which was treated with 5 mg/kg $CuCl_2$ prior to treatment with CS790AM. Importantly, $CuCl_2$ was injected 2 h before CS790AM to allow adequate time for absorption of Cu^{2+} into tissues and its reduction to Cu^+ (54). In mice pretreated with $CuCl_2$, we observe a *ca.* 60% increase in fluorescence relative to control mice, establishing that CS790AM can detect increases in

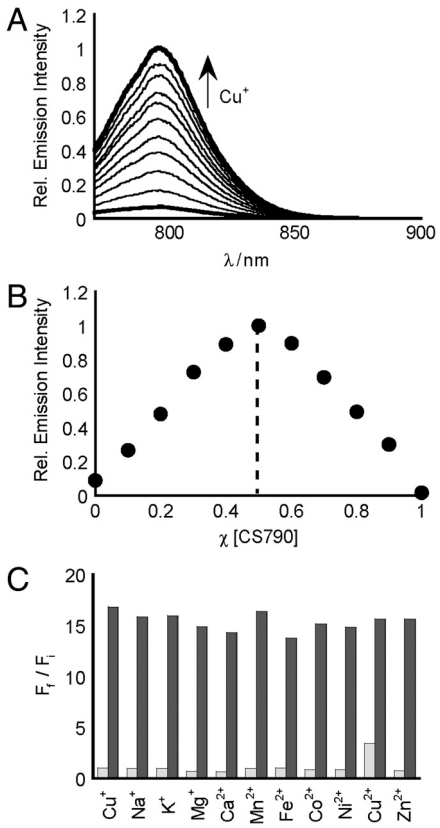

Fig. 2. Spectroscopic characterization of CS790. All spectra were acquired in 20 mM Hepes, pH 7.0, at 25 °C. (*A*) Fluorescence response of 2 μM CS790 to 0–2 μM Cu^{+}. Spectra shown are for [Cu^{+}] of 0, 0.2, 0.4, 0.6, 0.8, 1.0, 1.2, 1.4, 1.6, 1.8, and 2.0 μM. (*B*) Job's plot of CS790 and Cu^{+}. The total concentration of CS790C and Cu^{+} were kept at 2 μM, and spectra were acquired using a λ_{ex} of 760 nm and a λ_{em} of 790 nm. (*C*) Fluorescence responses of CS790 to various metal ions. Bars represent the final integrated fluorescence response (F_f) over the initial integrated emission (F_i). Light-gray bars represent the addition of an excess of the indicated metal ion (2 mM for Ca^{2+}, Mg^{2+}, and Zn^{2+}; 20 μM for all other cations) to a 2 μM solution of CS790. Dark-gray bars represent subsequent addition of 2 μM Cu^{+} to the solution. Excitation was provided at 760 nm and emission was recorded at 790 nm.

exchangeable Cu^{+} in living mice (Fig. 4). Alternatively, mice treated with 5 mg/kg Cu^{2+} immediately prior to CS790AM show no significant increases in fluorescence compared to control mice treated with CS790AM alone (Fig. S5), providing evidence that the fluorescence increase observed with copper pretreatment is due to detection of Cu^{+} generated from the reducing cellular environment. To determine the reversibility of copper binding in vivo, we utilized CS790AM imaging in mice injected with 5 mg/kg $CuCl_2$ as well as 5 mg/kg ATN-224 (55), a copper chelator. To our delight, the fluorescence from this set of mice was indistinguishable from mice injected with CS790AM alone, confirming that the copper-induced fluorescence enhancements in vivo can be reversed by competitive copper chelation (Fig. 4). Finally, we decreased basal levels of exchangeable copper in vivo by injecting mice with 5 mg/kg ATN-224 2 h prior to injection of CS790AM. The fluorescence from chelator-treated mice was significantly lower than the signal from mice treated with CS790AM alone, indicating that CS790AM can detect basal, endogenous levels of labile copper in living mice.

After demonstrating the ability of CS790AM to detect copper fluctuations in vivo, we sought to determine the correlation between whole-animal copper imaging with CS790AM and copper detection in internal tissues by an independent method. To

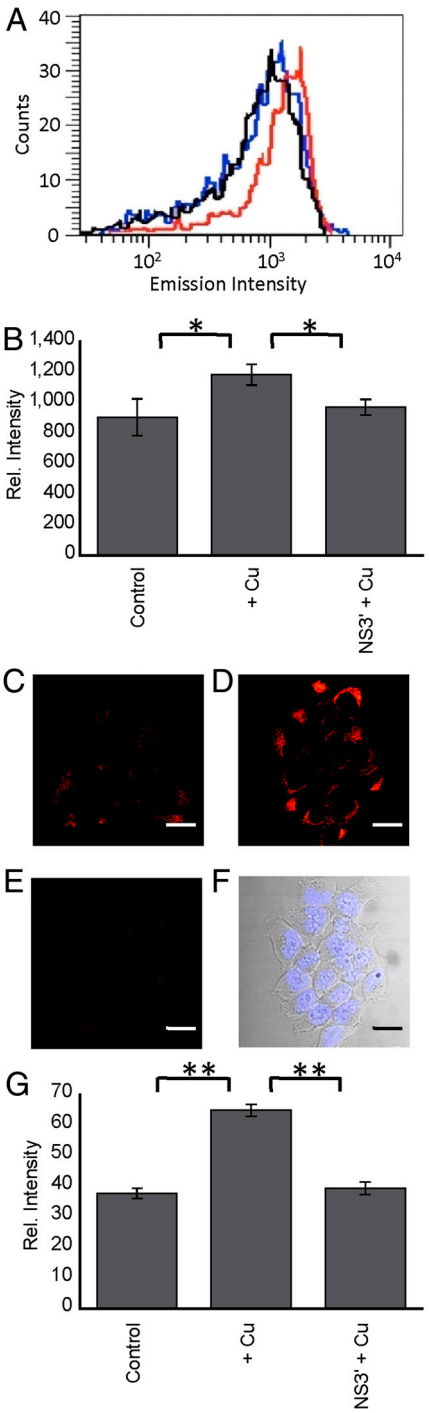

Fig. 3. Molecular imaging of Cu^{+} in HEK 293T cells. (*A*) Flow cytometry histograms for control cells (black), cells treated with 100 μM $CuCl_2$ for 12 h (red), and cells treated with 100 μM $CuCl_2$ for 12 h and 100 μM NS3′ (blue). For all conditions in *A*, cells were incubated with 2 μM CS790AM and NS3′ or vehicle for 15 min at 37 °C. (*B*) Graph showing quantification of mean fluorescence intensity of each condition shown in *A*, normalized to the control condition. (*C–F*) Confocal images of control cells (*C*), cells treated with 100 μM $CuCl_2$ for 12 h (*D*), cells treated with 100 μM $CuCl_2$ for 12 h and 100 μM NS3′ (*E*), and brightfield image of cells overlayed with the nuclear Hoechst 33342 stain, indicating cellular viability (*F*). *C–E* were stained with 2 μM CS790AM, 1 μM Hoechst 33342, and NS3′ or vehicle for 15 min at 37 °C. (Scale bar: 20 μm.) (*G*) Graph showing quantification of mean fluorescence intensity of each condition (*C–F*), normalized to the control condition. Statistical analyses were performed with a two-tailed Student's *t*-test. $*P < 0.05$ ($n = 3$), $**P < 0.001$ ($n = 3$). and error bars are ±SD.

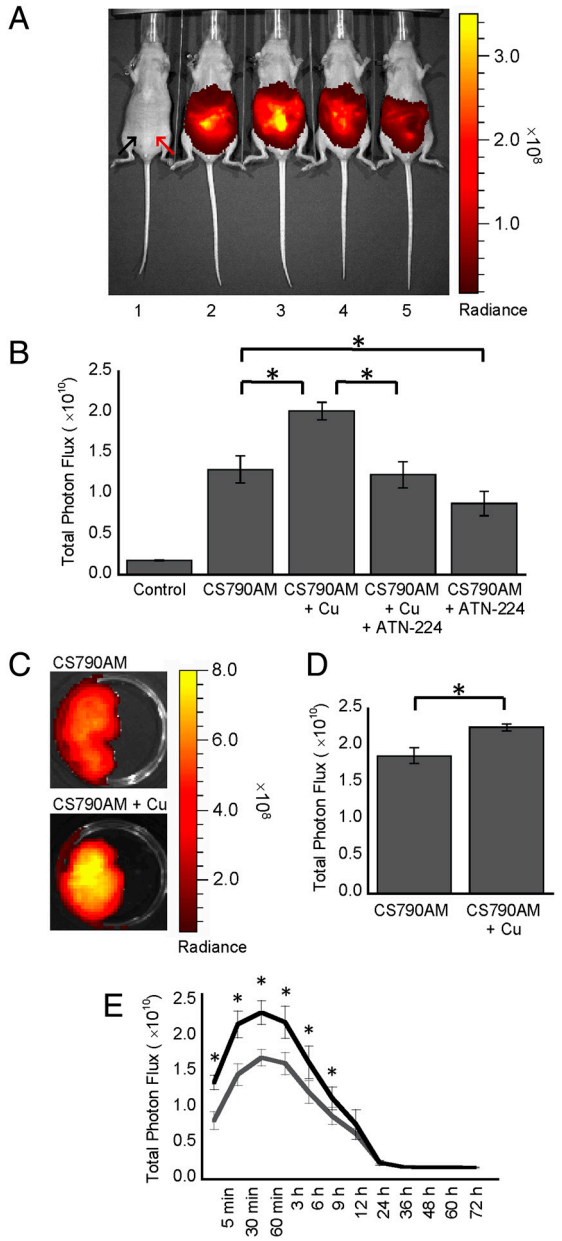

Fig. 4. CS790AM studies in SKH-1 mice. (*A*) Representative image of mice injected i.p. with vehicle, CS790AM (0.1 mM, 50 μL in 7:3 DMSO:PBS), $CuCl_2$ (5 mg/kg in 50 μL of PBS), and/or ATN-224 (5 mg/kg in 50 μL PBS). From left to right: vehicles only; vehicles and CS790AM; $CuCl_2$, vehicle, and CS790AM; $CuCl_2$, ATN-224, and CS790AM; vehicle, ATN-224, and CS790AM. For all mice, $CuCl_2$, ATN-224, or vehicle was injected 2 h prior to CS790AM or vehicle. Images were collected 5 min after CS790AM injection. Black arrow indicates injection location for $CuCl_2$, ATN-224, or vehicle; red arrow indicates injection location for CS790AM or vehicle. (*B*) Total photon flux from each mouse, 5 min after CS790AM injection. (*C*) Representative images of livers from SKH-1 mice injected i.p. with $CuCl_2$ or PBS, as described above, 2 h prior to CS790AM. (*D*) Total photon flux from imaged livers. (*E*) Fluorescence curves over 72 h for mice injected i.p. with $CuCl_2$ (black line) or PBS (gray line), as described above, 2 h prior to CS790AM. Statistical analyses were performed with a two-tailed Student's *t*-test. $*P < 0.05$ [$n = 3$ (*B* and *D*), $n = 4$ (*E*)] and error bars are ±SD.

this end, we pretreated mice with $CuCl_2$ or PBS 2 h prior to CS790AM and obtained fluorescence images of the whole animals to verify the detection of copper in vivo (Fig. S6). Mice were then perfused, and subsequent imaging of their livers replicated the fluorescence increase seen in vivo following copper treatment (Fig. 4). To quantitatively assess the total copper content in the livers, inductively coupled plasma mass spectrometry (ICP-MS) analysis was performed, which verified the copper increase seen after $CuCl_2$ injection (Fig. S6). Following these ex vivo studies, we sought to determine the lifetime of Cu^+ detection by CS790AM in mice and the corresponding clearance time for the sensor. To this end, mice were pretreated with PBS or $CuCl_2$ 2 h prior to treatment with CS790AM. Fluorescent imaging of these mice indicates that CS790AM has a robust response to Cu^+ for up to 9 h after injection (Fig. 4). Additionally, the fluorescent signal is fully attenuated within a few days (Fig. 4), providing a valuable opportunity for longitudinal monitoring of copper in a single mouse. Alternatively, fluorescent imaging of mice following simultaneous injection of $CuCl_2$ and CS790AM did not show increased fluorescence in Cu^{2+} treated animals, except for 12 h after the injections (Fig. S7), which indicates that CS790AM is best used for detection of Cu^+ levels that are present prior to dye injection.

CS790AM Visualizes Dynamic Changes in Exchangeable Copper Stores in a Murine Wilson Disease Model. After establishing that CS790AM can monitor fluctuations in exchangeable Cu^+ pools under copper depletion or overload as well as basal levels of labile copper in living mice, we sought to apply this unique chemical tool to study a disease model of copper misregulation. In this context, the *Atp7b*$^{-/-}$ mouse model is particularly attractive owing to its phenotypic and metabolic similarities to Wilson disease in humans and its preparation by targeted inactivation of a single gene, which ensures that any disease phenotypes reflect only the consequences of the loss of ATP7B function (14, 56–58). Specifically, a series of 7- to 11-wk-old WT and *Atp7b*$^{-/-}$ female mice were injected with CS790AM and imaged at 5, 30, and 60 min after injection. Comparison of fluorescent signals from the WT and *Atp7b*$^{-/-}$ mice indicates that the knockout mice exhibit higher levels of fluorescence compared to the WT mice, with statistically significant differences 30 min after CS790AM injection (Fig. 5). These data are in agreement with fluorescence measurements of the serum of CS790AM treated *Atp7b*$^{-/-}$ mice, which show increased CS790AM fluorescence compared to serum from heterozygote mice (Fig. S8). Importantly, the fluorescent signal in the serum coelutes with copper during gel filtration, verifying the detection of copper by CS790AM, even in complex mixtures (Fig. S8). Additionally, a separate group of *Atp7b*$^{-/-}$ mice was treated with vehicle or the copper chelator ATN-224, which is under development as a treatment for Wilson disease (55, 59). Following intraperitoneal injection of CS790AM, ex vivo imaging of livers from these mice indicates a decrease in fluorescence upon ATN-224 treatment (Fig. 5) with a corresponding decrease in the fluorescence to copper ratio in the serum (Fig. S8). To illustrate that the liver is indeed a major organ of copper accumulation, ICP-MS analysis of tissues was completed. As shown in Fig. S9, the *Atp7b*$^{-/-}$ mice exhibit an expected increase in liver copper compared to WT counterparts, but copper levels do not differ significantly in other tissue types. The results are consistent with the dominant expression of ATP7B in liver tissue and its essential functions in hepatic copper efflux. Taken together, these data demonstrate the ability of CS790AM to monitor in vivo alterations in exchangeable copper levels that result from a disease state as well as decreased copper levels following ATN-224 treatment of *Atp7b*$^{-/-}$ mice.

Concluding Remarks

The essential yet toxic nature of copper provides motivation for creating methods for noninvasive, real-time measurements of exchangeable, bioavailable copper pools in living systems. Whereas a growing number of chemical tools have been developed to probe copper biology at the cellular level, technologies that can illuminate the functions of this essential metal in whole animals remain limited. To meet this need, we have developed CS790, a first-generation near-IR turn-on fluorescent sensor for exchangeable copper stores in living cells and animals. Spectroscopic and

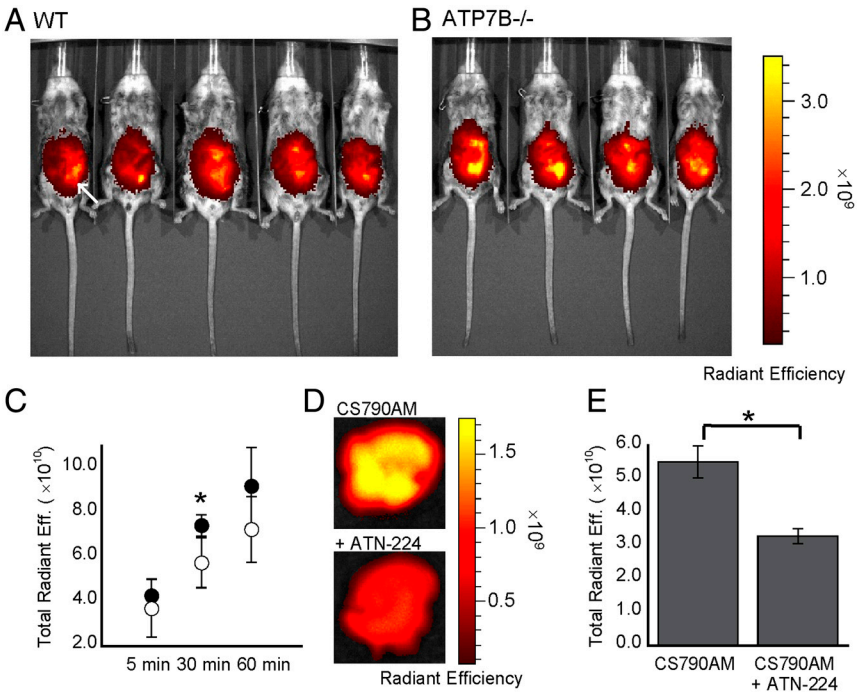

Fig. 5. CS790AM studies in *Atp7b*$^{-/-}$ mice. (*A* and *B*) Images of WT (*A*) and *Atp7b*$^{-/-}$ (*B*) mice 30 min after injection of CS790AM (0.1 mM, 50 μL in 7:3 DMSO : PBS). White arrow indicates location of CS790AM injection site. (*C*) Plot of total fluorescent signal from *Atp7b*$^{-/-}$ mice (black circles) and WT mice (white circles) 5, 30, and 60 min after CS790AM injection. (*D*) Representative images of livers from *Atp7b*$^{-/-}$ mice injected with PBS (i.p., 50 μL, *Upper*) or ATN-224 (i.p., 5 mg/kg in 50 μL PBS, *Lower*) 2 h prior to CS790AM. (*E*) Total photon flux from imaged livers. Statistical analyses were performed with a two-tailed Student's *t*-test. *$P < 0.05$ [$n = 5$ (*A*), $n = 4$ (*B*), $n = 2$ (*D*)] and error bars are ±SD.

live-cell imaging measurements establish the selectivity, sensitivity, and biological compatibility of the CS790 platform to monitor labile copper pools in vitro. Moreover, molecular imaging experiments in living mice clearly demonstrate the ability of CS790AM to report dynamic copper fluctuations in vivo and reveal that this probe is capable of detecting basal, endogenous levels of exchangeable copper in living mice. Notably, CS790AM has no apparent toxicity and is cleared from mice within a few days, thus providing the opportunity to monitor labile copper changes in a single mouse over time through various stages of health and disease. Indeed, additional work with a murine model of Wilson disease highlights the utility of CS790AM for detection of aberrant copper accumulation during pathological development, through the imaging of *Atp7b*$^{-/-}$ mice. Additionally, CS790AM monitoring of chelation treatment in *Atp7b*$^{-/-}$ mice further emphasizes the abilities of CS790AM for analysis of disease progression. Taken together, the results show that CS790AM can visualize fluctuations in bioavailable copper in living animals, affording a complementary technique to positron emission tomography of copper stores using radioactive ^{64}Cu (60, 61). The in vivo fluorescence detection of copper provided by CS790AM and related new chemical tools opens up unique opportunities to explore the roles that copper plays in healthy physiology as well as in the development and progression of disease.

Materials and Methods

Full materials and procedures for the synthesis of compounds, spectroscopic characterization, cellular imaging, and animal experiments are described in the *SI Text*.

ACKNOWLEDGMENTS. We thank Ann Fischer at the University of California, Berkeley (UCB) Tissue Culture Facility for her help with culturing the HEK 293T cells and Andrew Mazar (Northwestern University, Evanston, IL) for generously providing ATN-224. We thank the Packard Foundation (C.J.C.), Amgen (C.J.C.), Astra Zeneca (C.J.C.), Novartis (C.J.C.), and the National Institute of General Medical Sciences [National Institutes of Health (NIH) GM 79465 to C.J.C. and National Institute of Diabetes and Digestive and Kidney Diseases (NIDDK) DK084510 to S.L.] for funding this work. T.H. acknowledges the Japan Society for the Promotion of Science for a Postdoctoral Research Fellowship, and G.C.V.d.B. thanks UCB for a Klaus and Mary Ann Saegebarth Fellowship in Chemistry. L.W.G. acknowledges the NIH for a Predoctoral Fellowship (NIDDK F31 National Research Service Award DK084730-03). C.J.C. is an Investigator with The Howard Hughes Medical Institute.

1. Lippard S, Berg JM (1994) *Principles of Bioinorganic Chemistry* (University Science Books, Mill Valley, CA).
2. Gray H, Stiefel EI, Valentine JS, Bertini I (2007) *Biological Inorganic Chemistry: Structure and Reactivity* (University Science Books, Mill Valley, CA).
3. Prohaska J, Gybina AA (2004) Intracellular copper transport in mammals. *J Nutr* 134:1003–1006.
4. Que E, Domaille DW, Chang CJ (2008) Metals in neurobiology: Probing their chemistry and biology with molecular imaging. *Chem Rev* 108:1517–1549.
5. Thiele DJ, Gitlin JD (2008) Assembling the pieces. *Nat Chem Biol* 4:145–147.
6. Davis AV, O'Halloran TV (2008) A place for thioether chemistry in cellular copper ion recognition and trafficking. *Nat Chem Biol* 4:148–151.
7. Robinson NJ, Winge DR (2010) Assembling the pieces. *Annu Rev Biochem* 79:537–562.
8. Finkel T, Serrano M, Blasco MA (2007) The common biology of cancer and ageing. *Nature* 448:767–774.
9. Looi YH, et al. (2008) Involvement of Nox2 NADPH oxidase in adverse cardiac remodeling after myocardial infarction. *Hypertension* 51:319–325.
10. Kim BE, et al. (2010) Cardiac copper deficiency activates a systemic signaling mechanism that communicates with the copper acquisition and storage organs. *Cell Metab* 11:353–363.
11. Kang YJ (2011) Copper and homocysteine in cardiovascular diseases. *Pharmacol Ther* 129:321–331.
12. Barnham KJ, Masters CL, Bush AI (2004) Neurodegenerative diseases and oxidative stress. *Nat Rev Drug Discov* 3:205–214.
13. Gaggelli E, Kozlowski H, Valensin D, Valensin G (2006) Copper homeostasis and neurodegenerative disorders (Alzheimer's, prion, and Parkinson's diseases and amyotrophic lateral sclerosis). *Chem Rev* 106:1995–2044.
14. Lutsenko S, Gupta A, Burkhead JL, Zuzel V (2008) Cellular multitasking: The dual role of human Cu-ATPases in cofactor delivery and intracellular copper balance. *Arch Biochem Biophys* 476:22–32.
15. Beckman J, Estevez AG, Crow JP, Barbeito L (2001) Superoxide dismutase and the death of motoneurons in ALS. *Trends Neurosci* 24:S15–S20.
16. Valentine J, Hart PJ (2003) Bioinorganic chemistry special feature: Misfolded CuZnSOD and amyotrophic lateral sclerosis. *Proc Natl Acad Sci USA* 100:3617–3622.

17. Brown D, Kozlowski H (2004) Biological inorganic and bioinorganic chemistry of neurodegeneration based on prion and Alzheimer diseases. *Dalton Trans* 1907–1917.
18. Millhauser G (2004) Copper binding in the prion protein. *Acc Chem Res* 37:79–85.
19. Camakaris J, Voskoboinik I, Mercer JF (1999) Molecular mechanisms of copper homeostasis. *Biochem Biophys Res Commun* 261:225–232.
20. Bertini I, Rosato A (2008) Menkes disease. *Cell Mol Life Sci* 65:89–91.
21. Kaler SG (2011) ATP7A-related copper transport diseases—emerging concepts and future trends. *Nat Rev Neurol* 7:15–29.
22. Cox D, Moore SD (2002) Copper transporting P-type ATPases and human disease. *J Bioenerg Biomembr* 34:333–338.
23. Leary S, et al. (2007) The human cytochrome c oxidase assembly factors SCO1 and SCO2 have regulatory roles in the maintenance of cellular copper homeostasis. *Cell Metab* 5:9–20.
24. Domaille D, Que EL, Chang CJ (2008) Synthetic fluorescent sensors for studying the cell biology of metals. *Nat Chem Biol* 4:168–175.
25. McRae R, Bagchi P, Sumalekshmy S, Fahrni CJ (2009) In situ imaging of metals in cells and tissues. *Chem Rev* 109:4780–4827.
26. Haas K, Franz KJ (2009) Application of metal coordination chemistry to explore and manipulate cell biology. *Chem Rev* 109:4921–4960.
27. Yang L, et al. (2005) Imaging of the intracellular topography of copper with a fluorescent sensor and by synchrotron X-ray fluorescence microscopy. *Proc Natl Acad Sci USA* 102:11179–11184.
28. Zeng L, et al. (2006) A selective turn-on fluorescent sensor for imaging copper in living cells. *J Am Chem Soc* 128:10–11.
29. Miller E, Zeng L, Domaille DW, Chang CJ (2006) Preparation and use of Coppersensor-1, a synthetic fluorophore for live-cell copper imaging. *Nat Protoc* 1:824–827.
30. Taki M, et al. (2010) Development of highly sensitive fluorescent probes for detection of intracellular copper(I) in living systems. *J Am Chem Soc* 132:5938–5939.
31. Domaille D, Zeng L, Chang CJ (2010) Visualizing ascorbate-triggered release of labile copper within living cells using a ratiometric fluorescent sensor. *J Am Chem Soc* 132:1194–1195.
32. Dodani S, et al. (2011) Calcium-dependent copper redistributions in neuronal cells revealed by a fluorescent copper sensor and X-ray fluorescence microscopy. *Proc Natl Acad Sci USA* 108:5980–5985.
33. Dodani S, et al. (2011) A targetable fluorescent sensor reveals that copper-deficient SCO1 and SCO2 patient cells prioritize mitochondrial copper homeostasis. *J Am Chem Soc* 133:8606–8616.
34. Lim CS, et al. (2011) A copper(I)-ion selective two-photon fluorescent probe for in vivo imaging. *Chem Commun* 47:7146–7148.
35. You Y, et al. (2011) Phosphorescent sensor for robust quantification of copper(II) ion. *J Am Chem Soc* 133:11488–11491.
36. Wegner S, et al. (2010) Dynamic copper(I) imaging in mammalian cells with a genetically encoded fluorescent copper(I) sensor. *J Am Chem Soc* 132:2567–2569.
37. Wegner S, Sun F, Hernandez N, He C (2011) The tightly regulated copper window in yeast. *Chem Commun* 47:2571–2573.
38. Liu J, Lu Y (2007) A DNAzyme catalytic beacon sensor for aramagnetic Cu^{2+} ions in aqueous solution with high sensitivity and selectivity. *J Am Chem Soc* 129:9838–9839.
39. Liu J, Lu Y (2007) Colorimetric Cu^{2+} detection with a ligation DNAzyme and nanoparticles. *Chem Commun* 4872–4874.
40. Quaranta D, et al. (2011) Mechanisms of contact-mediated killing of yeast cells on dry metallic copper surfaces. *Appl Environ Microbiol* 77:416–426.
41. Santo C, et al. (2011) Bacterial killing by dry metallic copper surfaces. *Appl Environ Microbiol* 77:794–802.
42. Weissleder R, Ntziachristos V (2003) Shedding light onto live molecular targets. *Nat Med* 9:123–128.
43. Frangioni J (2003) In vivo near-infrared fluorescence imaging. *Curr Opin Chem Biol* 7:626–634.
44. Sasaki E, et al. (2005) Highly sensitive near-infrared fluorescent probes for nitric oxide and their application to isolated organs. *J Am Chem Soc* 127:3684–3685.
45. Peng X, et al. (2005) Heptamethine cyanine dyes with a large stokes shift and strong fluorescence: A paradigm for excited-state intramolecular charge transfer. *J Am Chem Soc* 127:4170–4171.
46. Zhang Z, Achilefu S (2005) Design, synthesis and evaluation of near-infrared fluorescent pH indicators in a physiologically relevant range. *Chem Commun* 5887–5889.
47. Hilderbrand S, Weissleder R (2007) Optimized pH-responsive cyanine fluorochromes for detection of acidic environments. *Chem Commun* 2747–2749.
48. Hilderbrand S, Kelly KA, Niedre M, Weissleder R (2008) Near infrared fluorescence-based bacteriophage particles for ratiometric pH imaging. *Bioconjug Chem* 19:1635–1639.
49. Myochin T, et al. (2011) Rational design of ratiometric near-infrared fluorescent pH probes with various pKa values, based on aminocyanine. *J Am Chem Soc* 133:3401–3409.
50. Chaudhry A, et al. (2010) Kinetically controlled photoinduced electron transfer switching in Cu(I)-responsive fluorescent probes. *J Am Chem Soc* 132:737–747.
51. Chaudhry A, Mandal S, Hardcastle KI, Fahrni CJ (2011) High-contrast Cu(I)-selective fluorescent probes based on synergistic electronic and conformational switching. *Chem Sci* 2:1016–1024.
52. Tsien R (1981) A non-disruptive technique for loading calcium buffers and indicators into cells. *Nature* 290:527–528.
53. Marban E, et al. (1990) Quantification of $[Ca^{2+}]_i$ in perfused hearts. Critical evaluation of the 5F-BAPTA and nuclear magnetic resonance method as applied to the study of ischemia and reperfusion. *Circ Res* 66:1255–1267.
54. Meyer L, Durley AP, Prohaska JR, Harris ZL (2001) Copper transport and metabolism are normal in aceruloplasminemic mice. *J Biol Chem* 276:36857–36861.
55. Lee V, Schulman JM, Stiefel EI, Lee CC (2007) Reversible precipitation of bovine serum albumin by metal ions and synthesis, structure and reactivity of new tetrathiometallate chelating agents. *J Inorg Biochem* 101:1707–1718.
56. Buiakova O, et al. (1999) Null mutation of the murine ATP7B (Wilson disease) gene results in intracellular copper accumulation and late-onset hepatic nodular transformation. *Hum Mol Genet* 8:1665–1671.
57. Huster D, et al. (2006) Consequences of copper accumulation in the livers of the $Atp7b^{-/-}$ (Wilson disease gene) knockout mice. *Am J Pathol* 168:423–434.
58. Lutsenko S (2008) $Atp7b^{-/-}$ mice as a model for studies of Wilson's disease. *Biochem Soc Trans* 36:1233–1238.
59. Brewer GJ (2009) Zinc and tetrathiomolybdate for the treatment of Wilson's disease and the potential efficacy of anticopper therapy in a wide variety of diseases. *Metallomics* 1:199–206.
60. Smith SV (2004) Molecular imaging with copper-64. *J Inorg Biochem* 98:1874–1901.
61. Peng F, Lutsenko S, Sun X, Muzik O (2011) Positron emission tomography of copper metabolism in the $Atp7b^{-/-}$ knock-out mouse model of Wilson's disease. *Mol Imaging Biol*, DOI: 10.1007/s11307-011-0476-4.